Instability of extremal relativistic charged spheres

Peter Anninos*
University of California, Lawrence Livermore National Laboratory, Livermore, California 94550

Tony Rothman†
Department of Physics, Bryn Mawr College, 101 North Merion Avenue, Bryn Mawr, Pennsylvania 19010

(Received 14 August 2001; published 29 November 2001)

With the question ''Can relativistic charged spheres form extremal black holes?'' in mind, we investigate the properties of such spheres from a classical point of view. The investigation is carried out numerically by integrating the Oppenheimer-Volkov equation for relativistic charged fluid spheres and finding interior Reissner-Nordström solutions for these objects. We consider both constant density and adiabatic equations of state, as well as several possible charge distributions, and examine stability by both a normal mode and an energy analysis. In all cases, the stability limit for these spheres lies between the extremal ($Q=M$) limit and the black hole limit ($R=R_+$). That is, we find that charged spheres undergo gravitational collapse before they reach $Q=M$, suggesting that extremal Reissner-Nordström black holes produced by collapse are ruled out. A general proof of this statement would support a strong form of the cosmic censorship hypothesis, excluding not only stable naked singularities, but stable extremal black holes. The numerical results also indicate that although the interior mass-energy $m(R)$ obeys the usual $m/R<4/9$ stability limit for the Schwarzschild interior solution, the gravitational mass M does not. Indeed, the stability limit approaches R_+ as $Q\rightarrow M$. In the Appendix we also argue that Hawking radiation will not lead to an extremal Reissner-Nordström black hole. All our results are consistent with the third law of black hole dynamics, as currently understood.

DOI: 10.1103/PhysRevD.65.024003 PACS number(s): 04.70.Bw, 97.60.Lf

I. INTRODUCTION

Extremal black holes, black holes for which the charge or angular momentum parameter equals the mass, occupy an exceptional position in black hole thermodynamics: due to their vanishing surface gravity they represent the absolute zero state of black hole physics. Over the past five or six years, compelling evidence has accumulated that extremal black holes represent a fundamentally different class of objects than their nonextremal counterparts. In some respects this is not surprising because the horizon structure changes completely at extremality (see, e.g. [1]) and all the thermodynamic properties of black holes depend on the horizon structure. The exact nature of extremality is still the subject of some debate. Semiclassical calculations for eternal, extremal black holes [2,3] indicate that the entropy is zero, while more recent semiclassical calculations for extremal objects collapsing into black holes [4,5] find that the temperature, and hence entropy, is not well defined. Similar results have been found for Bañados-Teitelboim-Zanelli (BTZ) black holes [6]. String theory calculations for extremal black holes, on the other hand [7], have yielded the ordinary Bekenstein-Hawking value for the entropy.

Given the pathological properties of extremal black holes, at least from the semiclassical side, one reasonable supposition is that such objects are, for reasons as yet unclear, disallowed by nature. Israel [8], for example, has proven a form of the third law, which shows that it is impossible to reach extremality by any finite-time, continuous accretion process (with some caveats). On the other hand, some simple solutions of the Einstein equations for extremally charged objects are known [9–11]. These studies, however, consider the rather unrealistic scenario of collapsing, infinitely thin shells. Moreover, the extremal solutions are evidently unstable, which again casts doubt on their relevance as models for genuine physical objects.

In this paper, we take a purely classical point of view and consider the stability of charged, spherical matter distributions that satisfy the Einstein equations. Essentially we investigate interior Reissner-Nordström solutions, focusing on the extremal $Q=M$ case. A study of relativistic charged spheres was undertaken thirty years ago by Bekenstein [12], but without numerics he was unable to reach many firm conclusions about the ability of charge to prohibit collapse. More recently a numerical investigation has been carried out by de Felice Siming and Yunqiang. [13] (dFSY). The dFSY study was limited in that it considered only spheres with constant matter density ρ and a power-law charge distribution. Furthermore, although ρ was taken to be constant in deriving the equation of hydrostatic equilibrium, the stability analysis assumed an adiabatic equation of state, i.e., $p\propto\rho_{rm}^{\gamma}$, where ρ_{rm} is the rest mass density. As will become clear below, the $\rho=$const case is the only convenient one for numerical integration; nevertheless, it is possible to construct a scheme capable of handling the more general adiabatic equation of state, as well as other charge distributions. We have done this for the present study and find that in all cases examined, instability sets in before extremality is reached.

II. EINSTEIN AND OPPENHEIMER-VOLKOV EQUATIONS FOR CHARGED SPHERES

To derive the relativistic hydro- and electro-dynamic equations for a charged fluid sphere, we assume a general

*Electronic address: anninos1@llnl.gov
†Electronic address: trothman@brynmawr.edu

 ©2001 The American Physical Society

spherically symmetric metric in the form

$$ds^2 = -e^{2\Phi}\mathrm{d}t^2 + e^{2\Lambda}dr^2 + r^2\mathrm{d}\theta^2 + r^2\sin^2\theta d\phi^2, \quad (2.1)$$

where $\Phi = \Phi_0(r) + \Phi_1(r,t)$ and $\Lambda = \Lambda_0(r) + \Lambda_1(r,t)$. In this section we are concerned only with the zeroeth-order (static) Einstein equations and so set $\Phi_1 = \Lambda_1 = 0$. The first-order quantities will be employed for the stability analysis in Sec. IV. We write the Einstein equations in the form

$$G_{\mu\nu} \equiv R_{\mu\nu} - \frac{1}{2}g_{\mu\nu}R = 8\pi T_{\mu\nu}, \quad (2.2)$$

with $c = G = 1$. For charged spheres, the energy-momentum tensor will consist of a perfect-fluid part

$$(T_{\mu\nu})_{hydro} = (\rho + p)u_\mu u_\nu + p g_{\mu\nu} \quad (2.3)$$

plus an electromagnetic part

$$4\pi(T_{\mu\nu})_{EM} = F^\alpha_\mu F_{\nu\alpha} - \frac{1}{4}g_{\mu\nu}F_{\alpha\beta}F^{\alpha\beta}. \quad (2.4)$$

In these expressions $\rho = \rho_{rm} + e$ is the total mass density, ρ_{rm} is the rest mass density, e is the internal energy density, p is the fluid pressure, u_μ is the four-velocity, and $F_{\mu\nu}$ is the electromagnetic field strength tensor. As in the derivation of the exterior Reissner-Nordström solution, we take the magnetic field B to be zero. Due to spherical symmetry, the electric field E must be entirely radial and the electromagnetic field tensor $F_{\mu\nu}$, which has only two components, $F_{01} = -E$ and $F_{10} = E$, must satisfy the Maxwell equations

$$\frac{1}{\sqrt{-g}}(\sqrt{-g}F^{\mu\nu})_{,\nu} = 4\pi j^\mu, \quad (2.5)$$

where j^μ is the four-current. The only nonvanishing derivative for the static case is $\nu = r$. Working out Eq. (2.5) gives

$$E(r) = \frac{e^{\Phi(r)+\Lambda(r)}Q(r)}{r^2}, \quad (2.6)$$

where

$$Q(r) \equiv 4\pi\int_0^r e^{\Phi(r')+\Lambda(r')}r'^2 j^0(r')dr'. \quad (2.7)$$

Equation (2.6) immediately implies

$$F^{01} = \frac{e^{-(\Phi(r)+\Lambda(r))}Q(r)}{r^2}. \quad (2.8)$$

Note that Eqs. (2.6) and (2.8) are of exactly the same form as the exterior Reissner-Nordström solution, as they must be by Gauss' law. The only difference is that for the interior case Q represents $Q(r)$ rather than the total charge. $(T_{\mu\nu})_{EM}$ must also be of the standard Reissner-Nordström form, or from Eqs. (2.4) and (2.8)

$$(T_{\mu\nu})_{EM} = \frac{Q^2(r)}{8\pi r^4}\mathrm{diag}[e^{2\Phi}, -e^{2\Lambda}, r^2, r^2\sin^2\theta]. \quad (2.9)$$

Also note that $T_{EM} \equiv (T^\mu_\mu)_{EM} = 0$ due to the antisymmetry of $F_{\mu\nu}$.

The left-hand side of the Einstein equations are the same as for any static, spherically symmetric solution. With the above expressions for $T_{\mu\nu}$, the (00) equation is found to be

$$\frac{1}{r^2} + \frac{2\Lambda' e^{-2\Lambda}}{r} - \frac{e^{-2\Lambda}}{r^2} = 8\pi\rho + \frac{Q^2}{r^4}, \quad (2.10)$$

and the (11) equation is

$$\frac{1}{r^2} - \frac{2\Phi' e^{-2\Lambda}}{r} - \frac{e^{-2\Lambda}}{r^2} = \frac{Q^2}{r^4} - 8\pi p, \quad (2.11)$$

where $(')$ denotes derivative with respect to r.

If one multiplies Eq. (2.10) by r^2, one gets

$$\frac{d(e^{-2\Lambda}r)}{dr} = 1 - 8\pi\rho r^2 - \frac{Q^2(r)}{r^2},$$

or

$$e^{-2\Lambda} = 1 - \frac{2m(r)}{r} - \frac{\mathcal{F}(r)}{r}, \quad (2.12)$$

where

$$m(r) \equiv 4\pi\int_0^r \rho r'^2\, dr' \text{ and } \mathcal{F}(r) \equiv \int_0^r \frac{Q^2(r')}{r'^2}dr'.$$

In the case where ρ is a constant and Q is taken to obey a power law in r, these expressions reduce to those in dFSY. However, we will not restrict ourselves to this situation.

To eliminate the metric functions Φ and Λ and to get the basic hydrodynamic equations we consider the conservation laws $T^{\mu\nu}{}_{;\nu} = 0$. The fluid part is the same as can be found in the derivation of the ordinary Oppenheimer-Volkov equation (see, e.g. [14]) and is found to be

$$T^{rr}{}_{;r} = e^{-2\Lambda}[p' + \Phi'(\rho + p)]. \quad (2.13)$$

The electromagnetic part is found to be

$$(T^{rr}_{EM})_{;r} = -\frac{e^{-2\Lambda}QQ'}{4\pi r^4}.$$

Setting the sum of these terms to zero and solving for Φ' yields

$$\Phi' = \frac{1}{\rho + p}\left[\frac{QQ'}{4\pi r^4} - p'\right]. \quad (2.14)$$

Solving Eq. (2.11) for Φ' and inserting the result into Eq. (2.14) yields

$$-\frac{p'}{\rho+p}=-\frac{1}{2r}+e^{2\Lambda}\left[4\pi rp+\frac{1}{2r}-\frac{Q^2}{2r^3}\right]-\frac{QQ'}{4\pi r^4(\rho+p)}. \tag{2.15}$$

With the form (2.12) for $e^{-2\Lambda}$ and some rearrangement of terms this can be written as

$$p'=\frac{QQ'}{4\pi r^4}-\frac{(\rho+p)}{r^2}\left[4\pi r^3p+m(r)+\frac{\mathcal{F}}{2}-\frac{Q^2}{2r}\right]\times\left(1-\frac{2m(r)}{r}-\frac{\mathcal{F}}{r}\right)^{-1}. \tag{2.16}$$

This is the Oppenheimer-Volkov (OV) equation for relativistic charged spheres, which will be the basis for our analysis.

We point out that the Newtonian version of this equation is

$$p'=\frac{QQ'}{4\pi r^4}-\frac{\rho m(r)}{r^2},$$

which shows that in the Newtonian limit the Coulomb repulsion opposes the gravitational force, as expected, helping to stabilize charged spheres against collapse. However in the relativistic OV equation with power-law charge distribution $Q\sim r^k$, $\mathcal{F}/2-Q^2/(2r)<0$. Thus these terms decrease the effective mass in the numerator of the second term, tending to ''stabilize.'' At the same time charge decreases the denominator, tending to ''destabilize.'' The final outcome is not entirely clear, which is why one needs to investigate the OV equation numerically.

III. INTEGRATION OF THE OPPENHEIMER-VOLKOV EQUATION

The basic strategy is simply to integrate Eq. (2.16) and test for the stability of solutions. Before doing this one must specify the charge distribution and an equation of state. We have no serious models of any sort for charged ''stars,'' or even know whether such objects exist. It seems intuitively reasonable that due to electrical repulsion the charge distribution should be weighted toward the surface, but otherwise all choices are basically *ad hoc*. One can imagine several plausible distributions. dFSY confined themselves to the simplest case, $Q\propto r^k$. We consider two distributions:

$$Q(r)=Q_T\left(\frac{r}{R}\right)^k e^{cr/R}\equiv\sqrt{\beta}r^k e^{cr/R}, \tag{3.1}$$

where R and β are adjustable input parameters that define the radius of the star and the total charge Q_T respectively, and

$$Q(r)=\sqrt{\beta}\tanh^k\left(\frac{r}{cR}\right), \tag{3.2}$$

which flattens out for $r\gg cR$. Note that in both these cases the charge density, obtained by differentiating Eq. (2.7), diverges at the origin unless $k\geqslant 3$. In point of fact, although we have been able to find solutions for the charge distribution (3.2), the stability analysis is generally inconclusive since no absolute boundary separation can be found consistently over all β of a given γ across the entire range of parameters considered here. The one exception is $\gamma=4$ in which case the results are qualitatively similar to the exponential distribution (3.1) for all β, and so we confine ourselves to that case.

Scarcely less arbitrariness applies to the equation of state (EOS) than to the charge distribution. Three obvious possibilities suggest themselves: $\rho=$const, the adiabatic EOS $p\propto\rho_{rm}^{\gamma}$ with arbitrary adiabatic index γ, and the ultrarelativistic EOS, $p=\rho/3$. However, despite the fact that an exact solution with infinite central density $\rho\propto r^{-2}$ for the last case is known when $Q=0$ (see [14]), we have found it difficult to find convergent solutions for this EOS when $Q\neq 0$ when iterating over central pressure. (This is as opposed to iterating over central density, which we do for arbitrary adiabatic index, below.) Thus we confine ourselves to the first two choices. We do, however, consider the $\gamma=4/3$ adiabatic EOS, which includes relativistic matter with non-negligible rest mass density (typically $\rho_{rm}/e\sim 10^2-10^4$ at the origin for $\gamma=4/3$, depending on p_c and β, and substantially lower ratios for larger γ). We reiterate that ρ represents the total mass-energy density of the matter plus gravitational field. Generally, the EOS is assumed to relate only the rest energy density, ρ_{rm}, and the pressure. As mentioned in Sec. II, the total local energy density is $\rho=\rho_{rm}+e$, where e is the internal energy density. We consider only polytropes, for which $e=p/(\gamma-1)$.

Once the charge distribution and EOS are specified we can integrate the OV equation. For virtually any case one can imagine, however, integrating Eq. (2.16) is impossible analytically and the integration must be carried out numerically. Even then, except for the case $\rho=$const, this turns out to be nontrivial. For $\rho=$const, the total mass will be simply $m(r)=(4/3)\pi r^3\rho$. With the boundary condition $p(R)=0$ and a form of Q to make $\mathcal{F}$ analytically integrable, this allows convenient integration from the outer boundary inward. For more reasonable equations of state, however, one expects ρ to vanish at $r=R$ as well [e.g., if $\rho=kp^{1/\gamma}+p/(\gamma-1)$]. In such cases the entire second term in Eq. (2.16) vanishes at the outer boundary, which causes a serious problem numerically because $dp/dr|_{r=R}=QQ'/(4\pi r^4)>0$, while $p(R-\Delta r)\approx -QQ'|\Delta r|/(4\pi R^4)$. Thus, unless $QQ'<0$, an inward integration scheme immediately predicts a negative pressure unless the integration is initiated from some arbitrary outer pressure and surface radius values to compensate for the charge distribution.

For this reason, we choose to integrate outwards from $r=0$. This strategy also presents difficulties. We can, say, choose R as the prespecified ''radius'' of the star, but in starting the integration at the origin, we have no prior knowledge of which combination of parameters ρ_c (central density), p_c (central pressure), γ, β, k, c, and Q will actually produce a star with radius R. In other words, if we define the physical surface radius R_p to be the point at which the pressure first goes negative, there is no reason that R_p will equal R. We have therefore adopted the following procedure: For a given

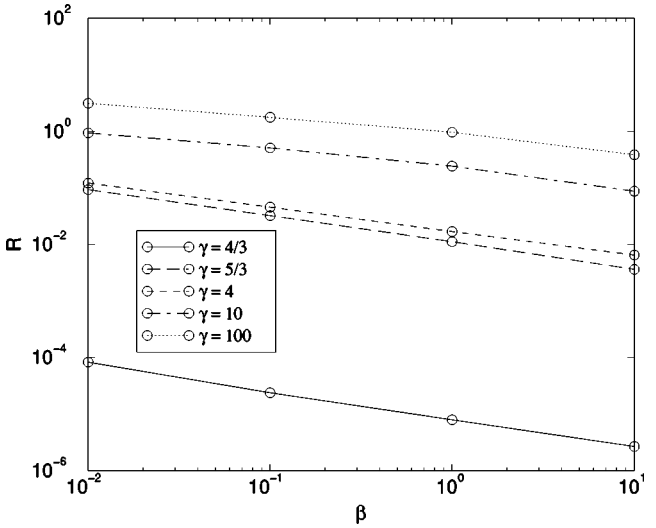

FIG. 1. Maximum surface radius as a function of charge parameter β found by converging in the central density to a tolerance of $\Delta\rho_c/\rho_c = 10^{-3}$ for a charge distribution $Q=\sqrt{\beta}r^3$ and the different adiabatic indexes considered in this paper. For fixed β, the numerical solutions do not converge to the specified tolerance at radii above the plotted curves.

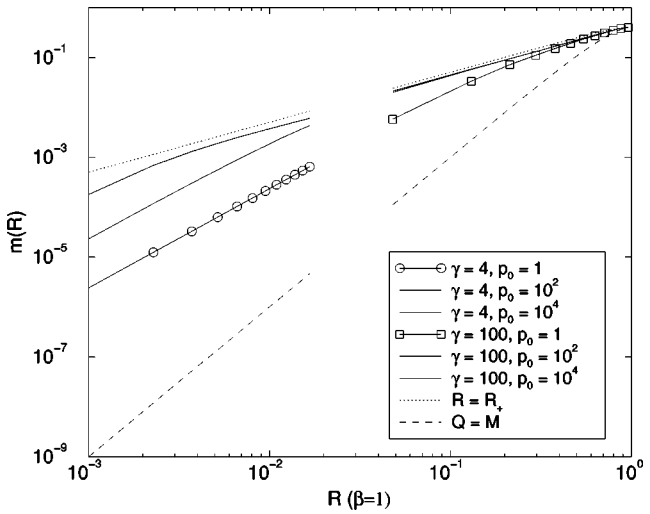

FIG. 2. Total mass density m as a function of outer surface radius R (up to $R=R_{max}$) for fixed charge parameter $\beta=1$. Each of the solid lines are solutions to the OV equations with different central pressures (the larger pressures correspond to greater mass densities). Also plotted are the densities for the corresponding black hole ($R=R_+$) and extremal charge ($Q=M$) limits.

parameter set $(R,\beta,\gamma,k,c,Q,\rho_c,p_c)$ we take a first guess at $\rho_c=1/(Rp_c^{1/\gamma})$ with arbitrary p_c, then iterate on ρ_c using a bisection algorithm until R_p converges to R. The bisection method assumes a locally monotonic correlation between $\delta\rho_c/\rho_c$ and $\delta R/R$, where the $(n+1)$-th estimate of the central density is given by $\rho_c^{(n+1)}=\rho_c^{(n)}+\delta\rho_c^{(n)}$. One chooses $\delta\rho_c^{(n)}$ by $\rho_c^{(n)}\delta R/R=\sigma\rho_c^{(n)}(R_p-R)/R$, where σ is a coefficient initially set to unity, but is halved for convergence whenever δR changes sign. We find in most cases we can converge on R to a relative tolerance of $\delta\rho/\rho\leqslant 0.1\%$.

The numerical integration is performed using an adaptive fourth order Runge-Kutta scheme to maintain a constant error tolerance of 10^{-12} over a grid constructed with cell spacing scaled to the surface radius such that $\Delta r/R\leqslant 5\times10^{-4}$. Further accuracy is achieved at the outer surface where pressure and density vary sharply by adaptively refining the mesh spacing to a minimum level $\Delta r\approx 10^{-12}$ when the pressure is observed to change sign. This procedure works well if R is sufficiently small. However, as R is increased one eventually hits a barrier $R=R_{max}$ beyond which convergence to the 0.1% tolerance is impossible or $(2m(r)+\mathcal{F})/r$ becomes so large that the metric function (2.12) becomes negative. This latter marks the black-hole limit $R=R_+=M+\sqrt{M^2-Q^2}$, where M is the exterior gravitational mass. The upper bound on R_{max} generally depends on all input parameters, and is computed numerically for each case presented in this paper. For example, considering an adiabatic EOS with $Q=\sqrt{\beta}r^3$, Fig. 1 shows the maximum surface radius as a function of β for the different γ considered in this paper. We are unable to find convergent solutions at radii above each of the curves.

Figure 2 plots the total mass $m(R)$ as a function of surface radius for $\gamma=4,100$ and fixed $\beta=1$. Here the surface radius is increased from 5% of R_{max} to the maximum computed value R_{max}. Each of the solid lines represent different central pressures p_c with the larger pressures resulting in greater masses. Also plotted in Fig. 2 are the corresponding black hole and extremal charge solutions for comparison. The black hole solution for $r=R$ is found by setting the metric function (2.12) equal to zero at that point, which gives $m(R)=(R-\mathcal{F}(R))/2$. By contrast, the extremal solution (not necessarily a black hole) is found by first matching the exterior Reissner-Nordström metric to the interior solution (2.1) at $r=R$:

$$1-\frac{2M}{R}+\frac{Q^2}{R^2}=\frac{1}{R}\int_0^R\left(1-8\pi\rho r^2-\frac{Q^2}{r^2}\right)dr \qquad (3.3)$$

which gives the definition of gravitational mass

$$M=\frac{1}{2}\int_0^R\left(8\pi\rho r^2+\frac{Q^2}{r^2}\right)dr+\frac{Q^2}{2R}. \qquad (3.4)$$

Setting $Q=M$ gives the extremal curve for $m(R)=4\pi\int\rho r^2dr$:

$$m(R)=Q-\frac{Q^2}{2R}-\frac{\mathcal{F}(R)}{2}. \qquad (3.5)$$

Finally we note that the total charge to total mass ratio Q/M generally increases monotonically with increasing R and fixed β, as Fig. 3 demonstrates. Since we are interested in the maximum or extremal limit of Q/M, the subsequent stability plots presented in Sec. IV are computed for those parameter values at the upper bounds of R $(=R_{max})$ for which we are able to find convergent solutions.

As a reminder, we point out that because we do not know beforehand the exterior mass of the star, the radius R in our

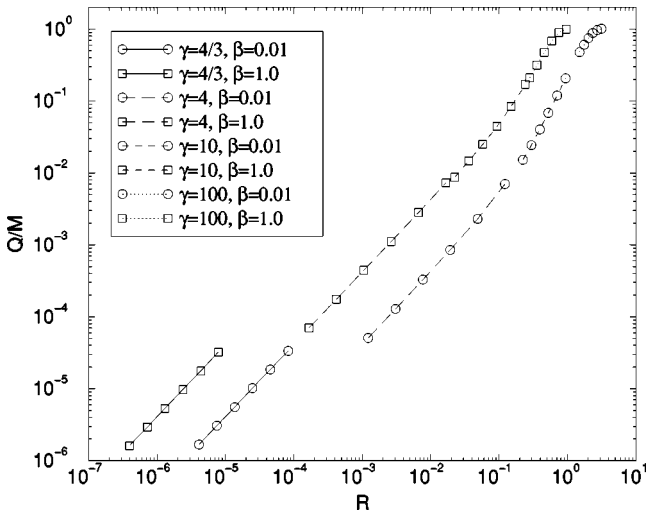

FIG. 3. Total charge to mass ratio Q/M is a monotonic function of surface radius up to the maximum computed radius R_{max}, and peaks at $Q\sim M$ for large γ. The results are shown for a central pressure $p_c=1$.

graphs is not given in units of M. R is merely where the pressure drops to zero expressed in geometric units.

IV. STABILITY I: NORMAL MODE ANALYSIS

We provide two stability analyses. The first, discussed in detail in this section, is a normal-mode analysis for radial pulsations of the charged sphere, similar to that performed by dFYS (see also [15] or [16]). The second, discussed in Sec. V, is based on the variation of energy.

We consider radial pulsations of the sphere with the goal of writing the Sturm-Liouville equation:

$$(F\zeta')'+(H+\omega^2 W)\zeta=0. \tag{4.1}$$

Here ζ is a ''renormalized displacement function,'' and F,H and W are functions of the zeroth-order (equilibrium) solution to the Einstein equations. ω is the angular frequency of the assumed sinusoidal time dependence of ζ. Once these functions are known, we evaluate

$$\omega^2=\frac{\int_0^R (F\tilde{\zeta}'^2-H\tilde{\zeta}^2)dr}{\int_0^R W\tilde{\zeta}^2\,dr}, \tag{4.2}$$

and deduce that the solution is stable under radial perturbations if $\omega^2>0$ for approximate trial functions $\tilde{\zeta}$ that satisfy the same boundary conditions as ζ.

To derive F, H, and W is a tedious undertaking; because we are now dealing with a time-dependent problem, the metric functions in Eq. (2.1) must be taken to be $\Phi=\Phi_0(r)+\Phi_1(r,t)$ and $\Lambda=\Lambda_0(r)+\Lambda_1(r,t)$, where we assume the first-order quantities are small. Once the perturbation equations are derived, to get the Sturm-Liouville form, the first-order quantities are eliminated in favor of the zeroth-order solutions. Nevertheless, because our equations differ slightly from dFYS, we now outline the procedure. The development basically follows that of Misner, Thorne, and Wheeler (MTW) [15], Chap. 26.

We first consider the total energy-momentum tensor. With the condition $g_{\mu\nu}u^\mu u^\nu=-1$, and raising and lowering with the full metric, one gets to first order $u_0=-e^{\Phi_0}(1+\Phi_1)$ and $u_1=e^{2\Lambda_0-\Phi_0}\dot{\xi}$, where $\xi(r,t)\ll r$ represents the small displacement of a fluid element initially at radius r. For the electromagnetic part of $T_{\mu\nu}$, we let $Q=Q_0+Q_1$, with $Q_1=-Q_0'(r)\xi(r,t)$ to first order. This is equivalent to assuming that the charge distribution in the oscillating system is the same as in the unperturbed system, i.e., that the Lagrangian perturbations vanish and no electric currents are introduced for the comoving observer. Then,

$$T_{00}=\left(\rho_0+\frac{Q_0^2}{8\pi r^4}\right)e^{2\Phi_0}+e^{2\Phi_0}\left(\rho_1+\Phi_1\left(\frac{Q_0^2}{4\pi r^4}+2\rho_0\right)-\frac{Q_0Q_0'\xi}{4\pi r^4}\right)$$

$$T_{01}=-e^{2\Lambda_0}(p_0+\rho_0)\dot{\xi}$$

$$T_{11}=\left(p_0-\frac{Q_0^2}{8\pi r^4}\right)e^{2\Lambda_0}+e^{2\Lambda_0}\left(p_1+\Lambda_1\left(2p_0-\frac{Q_0^2}{4\pi r^4}\right)+\frac{Q_0Q_0'\xi}{4\pi r^4}\right). \tag{4.3}$$

Note the presence of T_{01}, due to the fluid motion. This is entirely a first-order quantity.

The left-hand side of the Einstein equations are most easily computed with the help of MATHEMATICA or MAPLE. Then the (00) Einstein equation is found to be

$$\frac{e^{2\Phi_0}}{r^2}(1+2\Phi_1)+\frac{2}{r^2}e^{-2\Lambda_0+2\Phi_0}\left[-\frac{1}{2}+r\Lambda_0'+\Lambda_1(1-2r\Lambda_0')-\Phi_1(1-2r\Lambda_0')+r\Lambda_1'\right]$$

$$=8\pi e^{2\Phi_0}\left(\rho_0+\frac{Q_0^2}{8\pi r^4}\right)+8\pi e^{2\Phi_0}\left(\rho_1+2\Phi_1\left(\rho_0+\frac{Q_0^2}{8\pi r^4}\right)-\frac{2Q_0Q_0'\xi}{8\pi r^4}\right). \tag{4.4}$$

Equating orders on each side leads to the 0^{th}-order equation (2.10), which minus the charge term is also MTW Eq. (26.1b). The first-order equation, after some simplification, comes out to be

$$\frac{2e^{-2\Lambda_0}}{r^2}[\Lambda_1(1-2r\Lambda_0')+r\Lambda_1']=8\pi\rho_1-\frac{2Q_0Q_0'\xi}{r^4}. \tag{4.5}$$

With T_{01} given by Eq. (4.3), the (01) Einstein equation is then nontrivial and gives

$$\Lambda_1=-4\pi re^{2\Lambda_0}(p_0+\rho_0)\xi=-(\Lambda_0'+\Phi_0')\xi, \tag{4.6}$$

where the second equality follows from the zeroth-order equations (2.10) and (2.11).

We will shortly need an expression for the perturbed pressure p_1. One can get this from the law of baryon conservation $d(\Delta n)/d\tau=-n(\boldsymbol{\nabla}\cdot\mathbf{u})=(-g)^{-1/2}(\sqrt{-g}u^\alpha)_{,\alpha}$. Taking $\alpha=t,r$ yields

$$\Delta n=-n_0[r^{-2}e^{-\Lambda_0}(r^2e^{\Lambda_0}\xi)'+\Lambda_1], \tag{4.7}$$

where Δn represents the Lagrangian perturbation in n. Assuming adiabatic fluctuations such that $\Delta p/\Delta n=\gamma p/n$ then gives

$$p_1=-\gamma p_0[r^{-2}e^{-\Lambda_0}(r^2e^{\Lambda_0}\xi)'+\Lambda_1]-\xi p_0', \tag{4.8}$$

which is MTW Eq. (26.9).

The first-order (11) Einstein equation is found to be

$$\Phi_1'=4\pi re^{2\Lambda_0}\left(p_1+2\Lambda_1\left(p_0-\frac{Q_0^2}{8\pi r^4}\right)\right)+\frac{\Lambda_1e^{2\Lambda_0}}{r}+e^{2\Lambda_0}\frac{Q_0Q_0'\xi}{r^3}. \tag{4.9}$$

With Eqs. (4.6) and (4.8), Λ_1 and p_1 can be eliminated to get

$$\Phi_1'=-4\pi re^{2\Lambda_0}[\gamma p_0r^{-2}e^{-\Lambda_0}(r^2e^{\Lambda_0}\xi)']-4\pi re^{2\Lambda_0}\xi\left[p_0'+(\Lambda_0'+\Phi_0')\left(2p_0-\gamma p_0-\frac{Q_0^2}{4\pi r^4}+\frac{1}{4\pi r^2}\right)-\frac{Q_0Q_0'}{4\pi r^4}\right]. \tag{4.10}$$

By considering the parallel component of the conservation equation $u_\mu T^{\mu\nu}{}_{;\nu}=0$, using Eq. (4.7) and assuming the Lagrangian perturbation ΔQ vanishes, one can show

$$\rho_1=-(p_0+\rho_0)[r^{-2}e^{-\Lambda_0}(r^2e^{\Lambda_0}\xi)'+\Lambda_1]-\xi\rho_0', \tag{4.11}$$

which is MTW Eq. (26.11).

The transverse component of the conservation equation, $h^\mu_\nu T^\sigma{}_{\mu;\sigma}=0$, where the projection tensor $h^\mu_\nu=\delta^\mu_\nu+u^\mu u_\nu$ eventually yields

$$e^{2\Lambda_0-2\Phi_0}(\rho_0+p_0)\ddot{\xi}=-\Phi_0'(\rho_1+p_1)-\Phi_1'(\rho_0+p_0)-p_1'-\frac{1}{4\pi r^4}(Q_0'^2\xi+Q_0Q_0''\xi+Q_0Q_0'\xi'). \tag{4.12}$$

We note that the Q_0'' term does not appear in dFSY.

With these expressions we are finally able to write down the Sturm-Liouville equation. We define the renormalized displacement function $\zeta=r^2e^{-\Phi_0}\xi$ and assume $\zeta=\zeta(r)e^{-i\omega t}$. Then

$$F=\gamma p_0r^{-2}e^{\Lambda_0+3\Phi_0},$$

$$W=r^{-2}(\rho_0+p_0)e^{3\Lambda_0+\Phi_0},$$

$$H=r^{-2}e^{\Lambda_0+3\Phi_0}\left[4\pi r(\rho_0+p_0)e^{2\Lambda_0}\left(-p_0'+\frac{Q_0Q_0'}{4\pi r^4}+\frac{1}{r}(\rho_0+p_0)\right)+2p_0'\Phi_0'+p_0''+\Phi_0'\rho_0'-\frac{2p_0'}{r}-\frac{1}{4\pi r^4}\left(Q_0'^2+Q_0Q_0''+Q_0Q_0'\left(\Phi_0'-\frac{2}{r}\right)\right)\right]. \tag{4.13}$$

We have not attempted to reconcile this expression for H with the one in dFSY.

Physically reasonable solutions require ζ/r^3 finite or zero as $r\to0$ and $\gamma p_0r^{-2}e^{\Phi_0}\zeta'\to0$ as $r\to R$. Any trial function ζ that satisfies these conditions and that extremizes Eq. (4.2) is acceptable. Following Chandrasekhar and dFSY, we choose $\zeta\propto r^3$.

Figure 4 shows the stability curves for the adiabatic EOS with $Q=\sqrt{\beta}r^3$. The results are generated by choosing an initial central pressure (equal to unity) and iteratively solving the OV equation to convergence in the central density for fixed β and surface radius $R=R_{max}$. The central pressure is then monotonically increased and the OV equation repeatedly solved until the angular frequency defined in Eq. (4.2) becomes negative. The data points connected by solid lines are the solutions at which the frequency first becomes negative. Also shown are the black hole limit $R=R_+$ and the $Q=M$ limit, generated from Eq. (3.5). Note that the stability limit falls *between* the $Q=M$ curve and the black-hole curve. As can be seen from Fig. 3, Q/M varies over a broad range at $R=R_{max}$, but is constrained by $Q/M<1$ in the limit of large γ. Thus instability sets in *before* extremality is reached since Q/M decreases as the $R=R_+$ curve is approached (say by increasing the central pressure), even in the limit $\gamma\to\infty$ where all the curves come together.

Although for reasons of clarity we have not shown the $\gamma=4/3$ and 5/3 solutions in Fig. 4, they are qualitatively similar to the other cases, except that the extremal, stability and black hole curves are more widely separated. A more detailed plot of the $\gamma=100$ case is shown in Fig. 5 for two

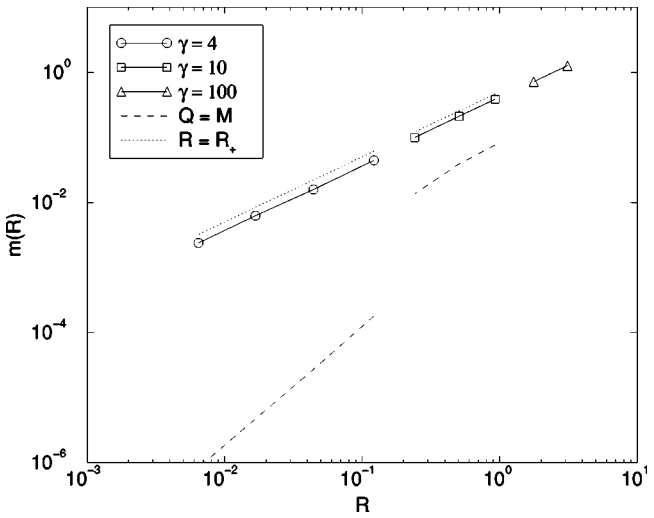

FIG. 4. Total mass function corresponding to the stability limit as a function of the maximum computed surface radius for $\gamma = 4,10,100$. The solid lines are found by increasing the central pressure from unity and plotting the first points which become unstable. The four points in the $\gamma=4$ curve represent for this distribution $Q=\sqrt{\beta}r^3$, $\beta=0.01,0.1,1.0,10$ (right to left). The three points for $\gamma=10$ represent $\beta=0.01,0.1,1.0$; the two points for $\gamma=100$ represent $\beta=0.01,0.1$. The displayed data are chosen to prevent overlap of the different γ curves, but we note that the general conclusion remains the same for all cases and choices of β investigated: the limit of stability lies between the $Q=M$ curves (dashed lines) and the black hole $R=R_+$ limit (dotted lines), even for $\gamma=4/3$ and 5/3 which are not shown here for clarity. Thus instability sets in before extremality is reached.

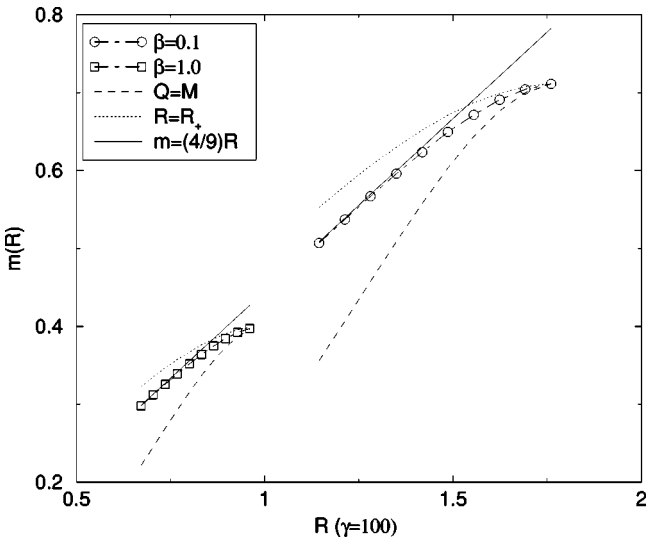

FIG. 5. As Fig. 4, except here we show closeups of the extremal, black hole, and stability curves for the more interesting high adiabatic index ($\gamma=100$) case over a range of surface radii leading up to the maximum $R=R_{max}$. Also plotted is the solid line $m(R)=4R/9$. The usual stability limit for the interior Schwarzschild solution is actually given by $M=4R/9$, where M is the gravitational mass. The two expressions are equivalent only in the limit $Q=0$; see also Fig. 6. In all cases, the stability curves separate the extremal charge and black hole states.

different values of β, and varying the surface radius up to $R=R_{max}$. Also shown in Fig. 5 with solid lines are the corresponding limits for the interior Schwarzschild solution when $Q=0$, $m(R)=4R/9$. This absolute limit is a good match to the numerically computed results even for relatively large ratios of Q/M and radii $R\sim R_{max}$. However, a more useful extension of this limit should employ the gravitational mass M deriving this constraint. Figure 6 plots the same result as 5, but for the gravitational mass $M(R)$. The solid lines are now the limits for the exterior Schwarzschild solution $M(R)=4R/9$. Notice that the upper bound of stability with this definition is always below, but approaches the black hole limit $R\rightarrow R_+\rightarrow M$ as $Q\rightarrow M$ and $R\rightarrow R_{max}$. This result is consistent with that of [17] who find no non-singular static solutions with $R\rightarrow R_+$ for $Q<M$.

The overall behavior is repeated in Figs. 7 and 8, which show similar graphs for two additional cases: the adiabatic EOS with $Q=\sqrt{\beta}r^3e^{r/R}$, and a constant density profile respectively. Once again, unstable solutions separate the $Q=M$ and black hole states. This is our main result: that the onset of instability always occurs before extremality is reached.

V. STABILITY II: ENERGY ANALYSIS

Admittedly, the above stability analysis is not exceptionally transparent. Somewhat more insight into the stability of relativistic charged spheres can be gained by considering an energy analysis. Following [16] and neglecting the electrostatic energy which is invariant with respect to changes in density, one can write the internal (thermal plus gravitational) energy of a spherical gas cloud as

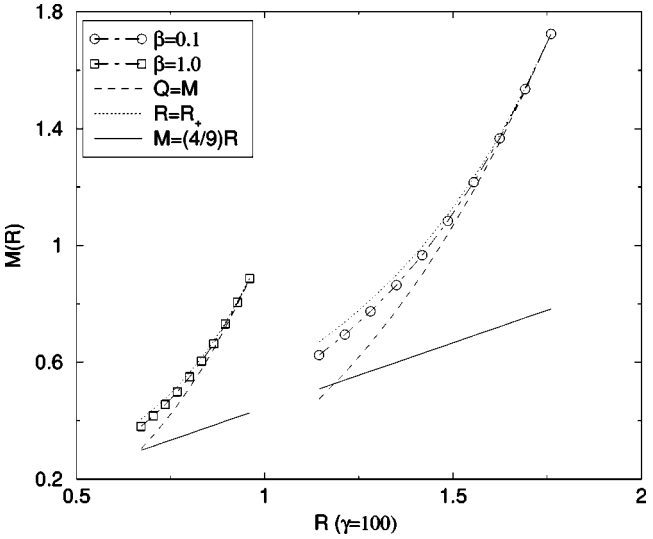

FIG. 6. As Fig. 5, except here we plot solutions for the gravitational mass M as a function of surface radius R. This time the solid lines show the stability limit $M(R)=4R/9$ for the interior Schwarzschild solution. Notice there is no absolute upper bound on stability other than the black hole limit $R\rightarrow M$ as $R\rightarrow R_{max}$ and $Q\rightarrow M$.

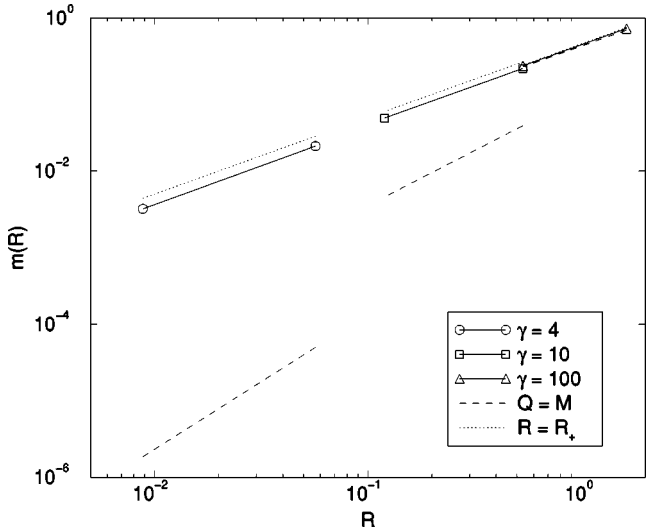

FIG. 7. As Fig. 4, but for a charge distribution of $Q=\sqrt{\beta}r^3e^{r/R}$. The symbols represent $\beta=0.01$ (right-most points) and 1.0 (left-most points).

$$E=\int_0^R\left[\rho\left(1-\frac{2m(r)}{r}-\frac{\mathcal{F}(r)}{r}\right)^{1/2}-\rho_{rm}\right]d\mathcal{V}, \qquad (5.1)$$

where the invariant volume element $d\mathcal{V}=4\pi(1-2m(r)/r-\mathcal{F}(r)/r)^{-1/2}r^2dr$. An equilibrium configuration is determined by the condition $\partial E/\partial\rho_{rmc}=0$, where ρ_{rmc} is the central rest-mass density, and the transition from a stable to unstable configuration is determined by the condition $\partial^2E/\partial\rho_{rmc}^2=0$ at the point where $\partial E/\partial\rho_{rmc}=0$. We find the transition numerically by first iteratively solving the OV equation for a given central pressure p_c until convergence is reached in ρ_c. The energy integral (5.1) is then evaluated

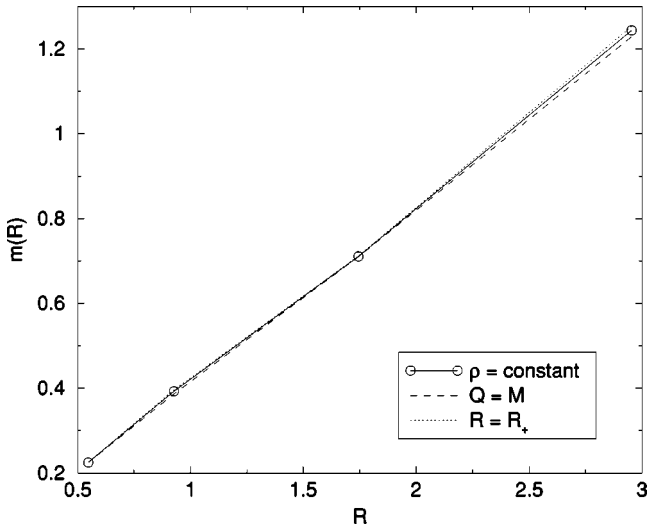

FIG. 8. As Fig. 4, but for a constant density distribution. The symbols represent $\beta=0.01,0.1,1.0,10$ (right to left). Although difficult to see, an unstable solution (sold line) always lies between the extremal and black hole curves for all surface radii $R\leqslant R_{max}$ we have studied. This figure is shown for $R=R_{max}$ as are most of the other stability plots.

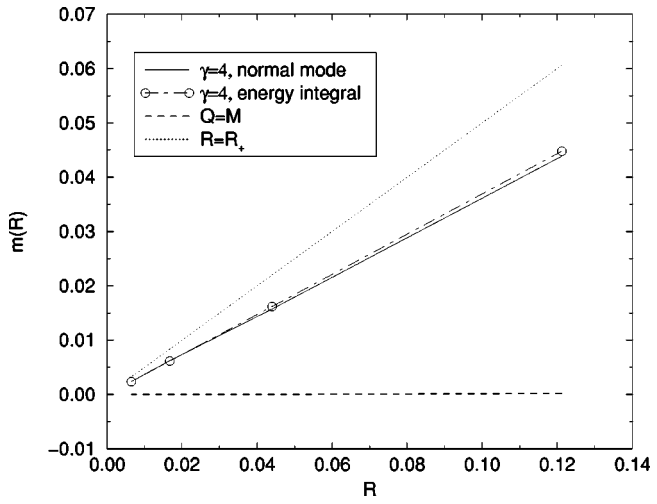

FIG. 9. Comparison of the energy variation and normal mode methods in evaluating the stability of solutions for the same $\gamma=4$ case as Fig. 4, but displayed on a linear-linear scale to distinguish the stability lines. Over the parameter range that both methods can be applied to reliably (mostly restricted by the energy method which is less robust from a numerical point of view), the results agree remarkably well.

and tabulated as a function of total mass and central rest-mass density. The inflection point is then easily computed as a function of M by discretizing the tabulated data with respect to ρ_{rmc}. Figure 9 shows a comparison of this method of evaluating stability with the normal mode analysis of Sec. IV for the $\gamma=4$ case of Fig. 4, but on a linear-linear scale. The results agree remakably well. However, we note that this energy approach is much more sensitive to numerical resolution and accuracy than the normal mode method. In fact, this method proves generally inconclusive for extreme (both small and large) values of γ. Hence we rely exclusively to the more robust normal mode method of Sec. IV to assess stability.

Equation (5.1) is already suggestive in that one can immediately see that the function $\mathcal{F}$ enters with the same sign as $m(r)$. In other words, charge effectively increases the magnitude of the gravitational potential energy, against the internal energy included in ρ, which should tend to destabilize the charged sphere. This can be confirmed by a perturbation analysis. Let $\rho=\rho_{rm}(1+u)$, where now u is the internal energy per unit mass, and assume that both $u\ll1$ and $m(r)/r\ll1$. Note that $\mathcal{F}/r\sim Q^2/r^2=(Q^2/m^2)(m^2/r^2)$, so this is at least a second order effect, $\mathcal{F}/r\sim m^2/r^2$ if $Q\sim m$, and even higher order if $Q\ll m$. Expanding Eq. (5.1) to lowest order in $\mathcal{F}$, gives

$$E=\int_0^R\rho_{rm}\left[u-\frac{m}{r}-\frac{um}{r}-\frac{m^2}{2r^2}-\frac{\mathcal{F}}{2r}\right]d\mathcal{V}. \qquad (5.2)$$

The first four terms are those found in computing the standard relativistic corrections to a Newtonian star (see [16], Chap. 6). The last term, which we denote as I_Q

$\equiv(1/2)\int \rho_{rm}(\mathcal{F}/r)d\mathcal{V}$ is the correction due to charge. Note that $I_Q \geqslant 0$ always. For a $\gamma=4/3$ polytrope one finds with the correction due to charge

$$E=(AM-BM^{5/3})\rho_{rmc}^{1/3}+CM\rho_{rmc}^{-1/3}-DM^{7/3}\rho_{rmc}^{2/3}-I_Q, \tag{5.3}$$

where A,B,C,D are positive numbers that depend on fundamental constants as well as on results of the numerical integration [see [16], Eq. (6.10.23)].

The condition $\partial E/\partial\rho_{rmc}=0$ gives

$$\frac{1}{3}(AM-BM^{5/3})\rho_{rmc}^{-2/3}-\frac{1}{3}CM\rho_{rmc}^{-4/3}-\frac{2}{3}DM^{7/3}\rho_{rmc}^{-1/3}-I_Q'=0. \tag{5.4}$$

Here, $I_Q' \equiv \partial I_Q/\partial\rho_{rmc} \approx (1/2)\int (a(r)\mathcal{F}/r)d\mathcal{V}$, where $a(r)$ represents the normalized density profile $\rho_{rm}=\rho_{rmc}a(r)$ with $a(r=0)=1$. We have also neglected higher order contributions from the invariant volume element $d\mathcal{V}$. For real stars, equating the first term in equation (5.4) to zero leads to the Chandrasekhar limit. The remaining terms are small corrections. Solving for the first term in the above equation and using the result in the condition $\partial^2 E/\partial\rho_{rmc}^2=0$ yields

$$\frac{2}{9}CM\rho_{rmc}^{-7/3}-\frac{2}{9}DM^{7/3}\rho_{rmc}^{-4/3}-\frac{2}{3}\rho_{rmc}^{-1}I_Q'=0. \tag{5.5}$$

To leading order $M\approx(A/B)^{3/2}$, so the onset of instability occurs at

$$C\left(\frac{A}{B}\right)^{3/2}-D\left(\frac{A}{B}\right)^{7/2}\rho_{crit}-3\rho_{crit}^{4/3}I_Q'=0. \tag{5.6}$$

When $I_Q=0$, this gives the standard result $\rho_{crit}=(C/D)(B/A)^2$. However, since $I_Q' \geqslant 0$, the presence of the last term clearly lowers ρ_{crit}, decreasing the threshold of instability by making the star unstable at lower densities and masses $m(r)$ at fixed R. This behavior is observed in Fig. 5 where as Q and Q/M are increased the stability curve falls further below the $R=(9/4)m(R)$ Schwarzschild stability limit. But, since we are increasing charge, we are increasing the gravitational mass M over $m(r)$ [see Eq. (3.4)], and so, paradoxically, when measured in M, the stability limit increases, as seen in Fig. 6.

VI. CONCLUSIONS

We have seen that, contrary to Newtonian intuition, in general relativity charge does not tend to stabilize or counterbalance the interior energy density of fluid spheres. To be sure, our numerical results indicate that for a fixed radius, instability sets in at a smaller mass $m(r)$ than in the fluid only case. Nevertheless, charge does increase the gravitational mass M, and the instability threshold for relativistic charged spheres monotonically approaches the black hole horizon in the extremal limit. Most important, though, for all cases studied the onset of instability of relativistic charged spheres takes place before the attainment of extremality. At that point, gravitational collapse into black holes takes place, but these are not extremal holes. All these results are certainly consistent with the currently accepted form of the third law of black hole dynamics, which forbids attainment of the extremal state by finite time processes involving accretion of positive energy [8] (see also Appendix).

One might legitimately doubt whether studies such as this one have any bearing on reality given that astrophysical objects tend not to be charged. For precisely this reason it has long been doubted that Reissner-Nordström solutions can represent astrophysical objects. On the other hand, to the extent that charged solutions shed light on the third law, they have been of great interest. Regardless, however, of whether one chooses to interpret charged spheres as stars or as solitons or as models for elementary particles, our results make it difficult to see how extremal objects could arise from any remotely realistic collapse scenario. A general theorem ruling out stable extremal black holes altogether would be desirable; it would effectively be an alternate formulation of the third law, as well as a strong version of the cosmic censorship hypothesis (or theorem, in that case); not only are stable naked singularities excluded, but stable extremal black holes as well.

Note added in proof. Since writing this paper we have learned that the results of the Appendix have also been achieved by S. Das *et al.* [20].

ACKNOWLEDGMENTS

We thank Werner Israel for an exchange that instigated the Appendix. This work was performed under the auspices of the U.S. Department of Energy by Lawrence Livermore National Laboratory of the University of California under Contract W-7405-Eng-48.

APPENDIX: A NOTE ON HAWKING RADIATION AND THE THIRD LAW

Israel's proof of the third law [8], that the surface gravity of a black hole can never be forced to zero in a finite-time, continuous process, assumed accreting charged shells and that the energy flux crossing the outer apparent horizon of the black hole was positive. Therefore the proof has nothing to say about Hawking radiation, because in this case a negative energy flux crosses the apparent horizon, violating the assumptions of the theorem. Moreover, at first glance, it might seem that Hawking radiation would drive a black hole toward extremality: If a black hole is emitting neutral particles, for example, the charge would remain constant while the mass decreased, forcing $Q/M\rightarrow 1$. It is not terribly difficult to see that this does not happen.

The power radiated by the black hole is

$$P=\frac{dM}{dt}\sim R^2T^4\sim R^2\kappa^4, \tag{A1}$$

where κ is the surface gravity. For a Schwarzschild black hole, $R=2M$ and $\kappa=1/4M$. This immediately gives the well known result for the evaporation time $\tau\sim M^3$.

For a Reissner-Nordström black hole, however, $R=R_+=M+\sqrt{M^2-Q^2}$ and the surface gravity is given by

$$\kappa = \frac{(M^2-Q^2)^{1/2}}{2M[M+(M^2-Q^2)^{1/2}]-Q^2} \tag{A2}$$

[see Wald [18], Eq. (12.5.4)]. Of course, as $Q \to M$, κ approaches zero, and therefore the flux, which goes as the fourth power of κ is rapidly decreasing. This suggests that an infinite amount of time is required to reach $Q=M$. The statement can be made rigorous by integrating Eq. (A1) for Reissner-Nordström black holes. With $R=R_+$ and the above expression for κ we have

$$\tau = \int \frac{[2M(M+\sqrt{M^2-Q^2})-Q^2]^4}{(M+\sqrt{M^2-Q^2})^2(M^2-Q^2)^2} dM, \tag{A3}$$

where the limits should be from M to Q, assuming $M>Q$ initially. With $Q=$const, the expression can be integrated analytically. The result for the indefinite integral is

$$\begin{aligned}\tau(M) = {} & \frac{32M^3}{3} + 16MQ^2 + \frac{MQ^4}{2(Q^2-M^2)} \\ & + \frac{2(16M^4+16M^2Q^2-41Q^4)}{3\sqrt{M^2-Q^2}} \\ & - \frac{35Q^3 \tanh^{-1}(M/Q)}{2}.\end{aligned} \tag{A4}$$

Assuming, for example, that $M_{initial} \gg Q$ and $M_{final}=Q(1+\epsilon)$ with $\epsilon<1$, then

$$\tau \sim \frac{64M^3}{3} + \frac{Q^3}{4\epsilon} + O(\epsilon^{-1/2}), \tag{A5}$$

which clearly diverges in the limit $Q \to M$ (equivalently $\epsilon \to 0$).

Although we have done this only for $Q=$const, it may hold true generally. If the Hawking temperature T is initially below the rest mass of the electron, the black hole will radiate only neutral particles and so Q will remain constant while M decreases. Plotting Eq. (A2) shows that κ and hence T will actually *increase* with decreasing mass until $Q=(\sqrt{3}/2)M$, at which point $\kappa=2/(9M)$ then monotonically decrease to zero as $\kappa \sim \sqrt{2\epsilon}/Q$ in the limit $M=Q(1+\epsilon)$. Assuming the maximum temperature is always less than the mass of the electron, then Q can be expected to remain constant, and evaporation cannot proceed in finite time, as discussed above.

If at any time T becomes greater than m_e, the hole will evaporate charge. But for any charged elementary particle $q \gg m$ due to negligible size of the gravitational interaction. Assuming that for temperatures above the rest mass, all species of particles are radiated with roughly equal probability (equipartition), under evaporation Q will become negligible compared to M and extremality will never be approached.

We emphasize that, as Israel points out, the entire discussion neglects any superradiant component which is nonthermal, but it is not clear whether this would alter the conclusion. We have also neglected other processes, such as discharge from pair production mentioned by Page [19], which in this case would likely only strengthen the conclusion. In any case, certainly for $Q=$const, Hawking radiation cannot violate the third law of black hole dynamics and perhaps not in general. This is consistent with the early work of Page and with the point of view that extremal black holes do not exist.

[1] S.W. Hawking and G.F.R. Ellis, *The Large-Scale Structure of Space-Time* (Cambridge University Press, Cambridge, England, 1973), p. 159.
[2] S.W. Hawking, G. Horowitz, and S.F. Ross, Phys. Rev. D **51**, 4302 (1995).
[3] C. Teitelboim, Phys. Rev. D **51**, 4315 (1995); **52**, 6201(E) (1995).
[4] S. Liberati, T. Rothman, and S. Sonego, Phys. Rev. D **62**, 024005 (2000).
[5] T. Rothman, Phys. Lett. A **273**, 303 (2000).
[6] A.J.M. Medved and G. Kunstatter, Phys. Rev. D **63**, 104005 (2001).
[7] A. Strominger and C. Vafa, Phys. Lett. B **379**, 99 (1996).
[8] W. Israel, Phys. Rev. Lett. **57**, 397 (1986).
[9] D.G. Boulware, Phys. Rev. D **8**, 2363 (1973).
[10] Ch.T. Farrugia and P. Haijeck, Commun. Math. Phys. **68**, 291 (1979).
[11] M. Proszynski, Gen. Relativ. Gravit. **15**, 403 (1983).
[12] J. Beckenstein, Phys. Rev. D **4**, 2185 (1971).
[13] F. de Felice, L. Siming, and Y. Yunqiang, gr-qc/9905099.
[14] Steven Weinberg, *Gravitation and Cosmology* (Wiley, New York, 1972), Chaps. 5, 11.
[15] C.W. Misner, K.S. Thorne, and J.A. Wheeler, *Gravitation* (Freeman New York, 1973), Chap. 26.
[16] S.L. Shapiro and S.A. Teukolsky, *Black Holes, White Dwarfs and Neutron Stars* (Wiley, New York, 1983), Chap. 6.
[17] Y. Yunqiang and L. Siming, gr-qc/9904050.
[18] Robert Wald, *General Relativity* (Chicago University Press, Chicago, 1985).
[19] D. Page, Phys. Rev. D **13**, 198 (1976); **14**, 3260 (1976).
[20] S. Das, A. Dasgupta, and P. Ramadevi, Mod. Phys. Lett. A **12**, 3067 (1997).